A new expression for fluid factor using AVO intercept and gradient: theory and application on deep marine reservoir

Mohammed Farfour[1] and John P. Castagna [2]
[1]Earth Science Dept., Sultan Qaboos University, Oman
[2]Department of Earth and Atmospheric science, University of Houston
Corresponding author: mfarfour@squ.edu.om

The work in the manuscript was presented in IMAGE21 (https://doi.org/10.1190/segam2021-3575102.1).

This is a non-peer-reviewed preprint submitted to EarthArXiv.

A slightly different version of this manuscript is submitted and accepted for publication in Interpretation.

Abstract

Numerous AVO fluid indicators have been introduced and proven to be sensitive to hydrocarbon presence. Mathematically, fluid indicators measure the deviation of seismic responses of hydrocarbon-saturated reservoirs from their background in a specific domain. We introduce a new expression for the fluid factor commonly used in AVO analysis and interpretation. The expression is a function of common AVO intercept and gradient and a weighting coefficient that helps suppressing the contribution of lithology and other factors not related to fluid content. The coefficient also assists in calibrating the fluid factor to the local geology. The performance of the proposed fluid factor is compared with other existing fluid factors. All the fluid factors are tested on a worldwide collection of P and S velocity and density measurements. The test is followed by an application on real data from the Northwest Shelf of Australia. Three wells are used in the application; two are used for calibration while the third is used as blind well. The fluid factor detects the gas zones at the three well locations and identifies prospects that have not been drilled.

Key words: AVO, gas-sand, seismic amplitude, Offshore

1. Introduction

Geological formations are characterized by their elastic properties such as P-wave and S-wave velocities (Vp and Vs), densities, Poisson ratio, shear modulus, bulk modulus, etc. (Farfour, 2020). In normal conditions, Vp, Vs, and density are often highly correlated (e.g., Castagna et al. 1998). The presence of hydrocarbons in porous rocks can cause observable deviations from this high correlation. Seismically, the deviation caused by fluids often results in abnormal seismic expressions that can help differentiate reservoir rocks from their background. Many papers have discussed the relationship between fluid and seismic amplitude (Koeffoed 1956; Ostrander 1984; Farfour et al. 2018; Farfour and Foster, 2022). For example, Koeffoed (1956) demonstrated that changes of Poisson ratio can result in a significant variation of amplitude. Domenico (1977), among others, showed that pore fluids significantly affect the dynamic Poisson's ratio. In other words, changes in fluid type cause changes in Poisson ratio which in turn causes variations in seismic amplitude. Ostrander (1984) and Smith and Gidlow (1987) have combined the above observations to demonstrate that the variations in amplitude with offset can be quantified and used as a hydrocarbon indictor.

The Zoeppritz equations are commonly used to compute amplitude at different angles of incidence. Bortfeld (1960) derived a useful approximation that separates acoustic and elastic contributions to reflectivity variation with angle. Aki and Richard (1980) simplified the Zoeppritz equation to a linear approximation in terms of P-wave velocity (Vp), S-wave velocity (Vs), and density reflectivities. Shuey (1985), on the other hand, suggested another approximation that involves Poisson ratio (or Vp/Vs), P-wave reflectivity, and density and separated AVO response into contributions from intercept (I) and gradient (G). Fatti et al. (1994) proposed different approximation as a function of P-wave reflectivity, S-wave reflectivity, and density reflectivity. Gray (2002) introduced an approximation expressing the seismic amplitude as a combination of Lamé parameters. Farfour and Foster (2021) reformulated the Shuey (1985) expression using Scaled Poisson Reflectivity and Gradient. The above linearized approximations helped invert the amplitude in prestack gathers for quantities attributable to fluid present in the rock. For example, the product I*G from Shuey's expression has been extensively utilized to identify unconsolidated gas sands. In addition, Smith and Gidlow (1987) have introduced two linear combinations of P-wave and S-wave reflectivity to detect fluid responses; the first was named scaled Poisson ratio, and the second is the fluid factor. We denote their fluid factor, here, as FF1. Fatti et al. (1994) have re-expressed FF1 and wrote it in a form of linear combination of P-wave and S-wave reflection coefficients at zero offset, Rp, and Rs; we denote this second version of the fluid factor by FF2. In this study, we present a new form of the Smith and Gidlow fluid factor; we denote it as FF3. Unlike FF1 and FF2, FF3 is expressed as a direct combination of the intercept and the

gradient. Similar to FF1 and FF2, FF3 can be used for all classes of sands. We compare FF3 against FF1 and FF2 using data collected from different world basins. We then apply the attribute on ~~a~~ real 3-D seismic data from North Western Australia.

2. Theory

The Zoeppritz approximation proposed by Shuey (1985) expresses reflection coefficients at different angles as a function of Vp for average Vp, Vs for average Vs, and ρ for average density:

$$R(\theta) \approx R_p + \left[\frac{\Delta Vp}{2Vp} - 4\frac{Vs^2}{Vp^2}\left(\frac{\Delta\rho}{2\rho} + \frac{\Delta Vs}{Vs}\right)\right]\sin^2\theta + \frac{\Delta Vp}{2Vp}(\tan^2\theta \sin^2\theta); \quad (1)$$

At angles less than 30 degrees, the equation above is commonly simplified to the form:

$$R(\theta) \approx I + G\sin^2\theta; \quad (2)$$

where I is the intercept or simply R_p which is defined as:
$I \approx \frac{\Delta Vp}{2Vp} + \frac{\Delta\rho}{2\rho}$; and G is the gradient.
Intercept I and the gradient G are typically obtained on real seismic data by fitting amplitude versus angle data from which other quantities can be derived.

Smith and Gidlow (1987) demonstrated that the fluid factor (FF1), once adjusted to local geology, could be an excellent indicator of hydrocarbons and more sensitive to hydrocarbon presence than other indicators. FF1 measures the deviation from a linear relationship between Vp and Vs such as the mud-rock line in the Vp-Vs domain (Castagna et al., 1985). FF1 is expressed as:

$$FF1 = \frac{\Delta Vp}{Vp} - g\frac{\Delta Vs}{Vs} \quad (3)$$

where $g = M * (V_s/V_p)$. M is the slope of the linear relationship but can also be varied to account for overburden effects.

The pseudo-Poisson's reflectivity R_σ introduced by Smith and Gidlow (1987) is defined as

$$R_\sigma = \frac{\Delta Vp}{Vp} - \frac{\Delta Vs}{Vs} \quad (4)$$

When V_s/V_p is close to 0.5, Castagna et al. (1994) demonstrated that:

$$R_p - R_s \approx (I + G)/2 \quad (5)$$

Substituting equation 5 into 4 gives

$$R_\sigma = I + G \quad (6)$$

Using equation 3 and 4, we can express FF1 as a function of R_σ as:

$$FF1 = R_\sigma - (g - 1)\frac{\Delta Vs}{Vs} \quad (7)$$

When density contrasts are small and at small angles (less than 30 degrees), the contribution of density is negligible compared to Vp and Vs. Thus,

$$\frac{\Delta Vs}{Vs} \approx I - G \quad (8)$$

Then, the fluid factor can then be written as

$$FF3 = (I + G) + (1 - g)(I - G) \quad (9)$$

One of the advantages of the above expression is that it will help produce the fluid factor directly from the intercept and gradient. As the case for the existing fluid factors (FF1 and FF2), FF3 requires the slope of the background line and the Vp/Vs ratio of the brine-saturated sand in the area. Both quantities can be determined from well data (Smith and Gidlow, 1987; Fatti et al. 1994). However, this will not account for overburden wave propagation effects or other amplitude scaling issues. In practice, g can also be estimated empirically using the intercept and gradient expression in equation 9. In next section, we show an example of how g can be determined.

3. Application on data samples

Petrophysical computations (absent amplitude scaling and wave propagation effects) of the three fluid factors FF1, FF2, and FF3 are examined on data samples collected from different areas around the globe (Castagna and Smith 1994). The samples involve Vp, Vs, and density information of gas-charged reservoirs, brine-saturated sands, and shale from each area. The data set involves 25 samples. We added 10 samples from Offshore Australia, Canada, and Middle East. We initially attempt to find best calibration parameter, g, for the three attributes. Smith and Sutherland (1994) show that the optimum value of g can be obtained by maximizing the performance function, Q, given by:

$$Q = \frac{\sum FF(gas\_sand/water\_sand) - \sum FF(shale/gas\_sand)}{|\sum FF(shale/water\_sand)|} \quad (10)$$

where FF is the fluid factor of interest.

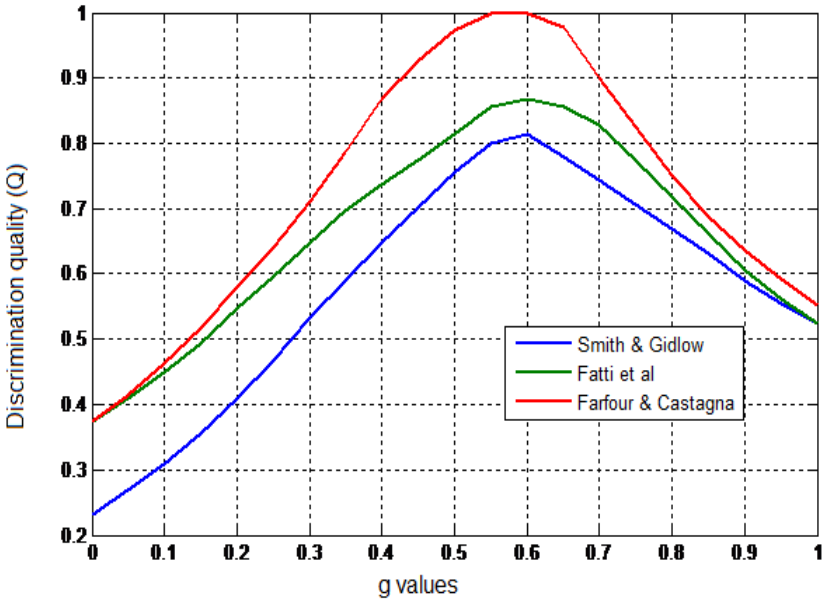

Fig. 1 The performance (Q) of the different fluid factors computed at different g values. Vertical axis represents normalized amplitude.

Figure 1 shows the performance of the fluid factors computed at different g values. We notice that all the fluid factors, FF1, FF2, and FF3, reach their best capability of fluid detection and discrimination at g values close to 0.6. In addition FF3 exhibits better performance than the FF2 and FF1 and reaches

To quantify and score the fluid discrimination capability of each attribute we used following formula:

$$S = \frac{|A_{sr}-A_{sb}|.|A_{rb}-A_{sb}|}{|A_{sb}|} \qquad (11)$$

where A_{sr} are the normalized values of attributes computed at the shale/reservoir interface; A_{sb} are the normalized values of attributes computed at shale/brine sand interface; A_{rb} are the normalized values of attributes at the reservoir/brine-sand interface. The scoring formula is proposed based on the Castagna and Smith (1994) definition for the ideal AVO attribute, which should exhibit large anomalies at the top and bottom of reservoirs with different signs. At the interface away from the reservoir zone, the attribute should be near zero and relatively invariant with depth. Note that the numerator terms in the formula should be both large and the denominator should be small for an attribute to score high.

Before assessing the performance of the three attributes we compare the attributes using common data analysis tools. The comparison may help demonstrate the link between the attributes and show the added value of the different versions of the fluid factor.

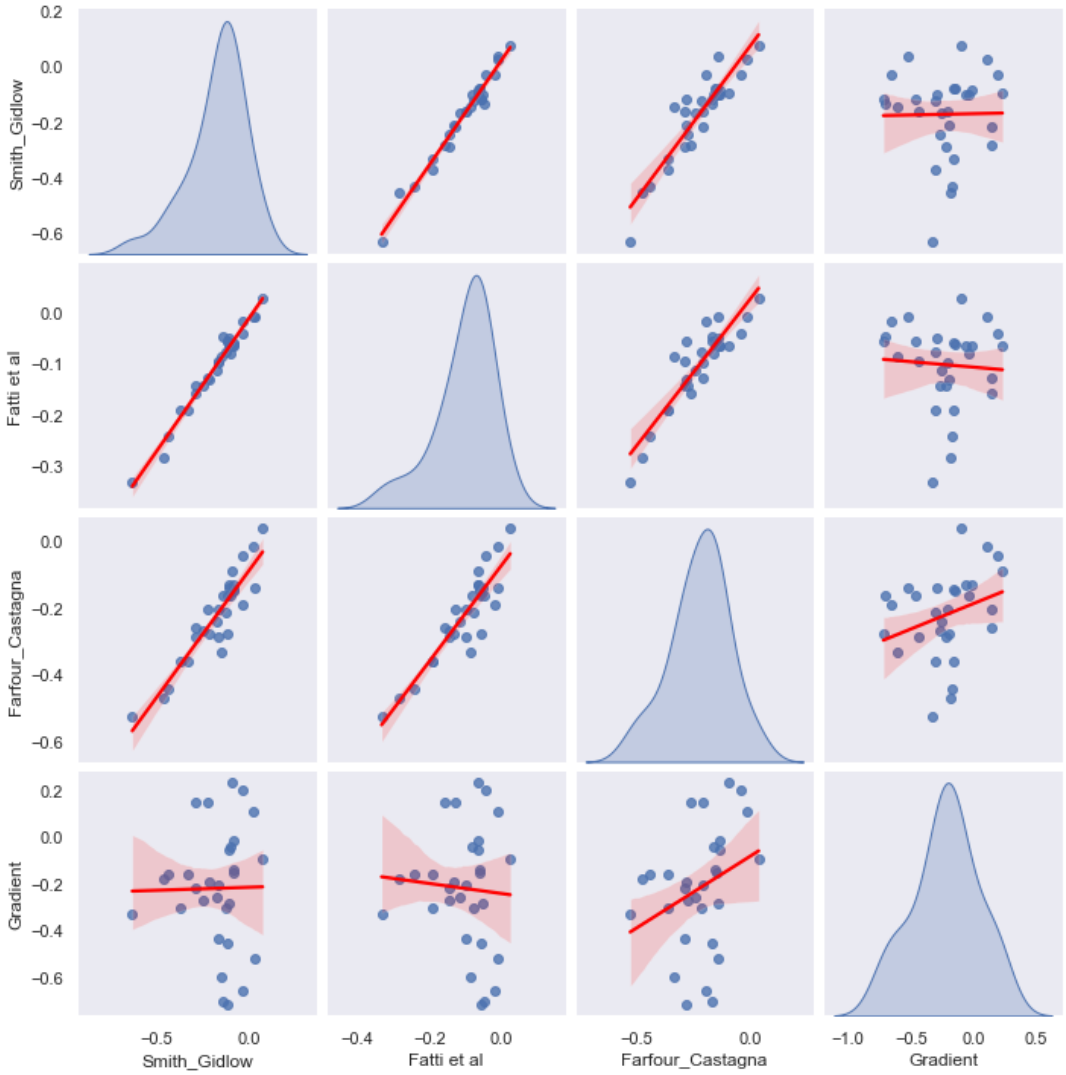

Fig. 2 Different cross-plots obtained from pair-plot showing the differences and similarity between fluid factors. Histograms show the normal distributions of the different factors.

The cross-plots between the fluid attributes demonstrate that they are different from the first AVO attribute used for fluid detection by Ostrander (1984), the Gradient. The Gradient commonly shows large amplitude changes due to fluid but cannot distinguish them from other geological factors such as lithology. The other attributes, with the help of the calibration parameter highlight only fluid and fluid-like anomalies. The pair-plot also suggests that attributes of Fatti and Simth and Gidlow have very high correlation. The main difference between the two attributes is that the Fatti et al. (1994) added the density term and expressed the attribute as a function of P and S waves' reflectivity instead of velocities. This high correlation indicates insensitivity of the attribute to typical density variations.

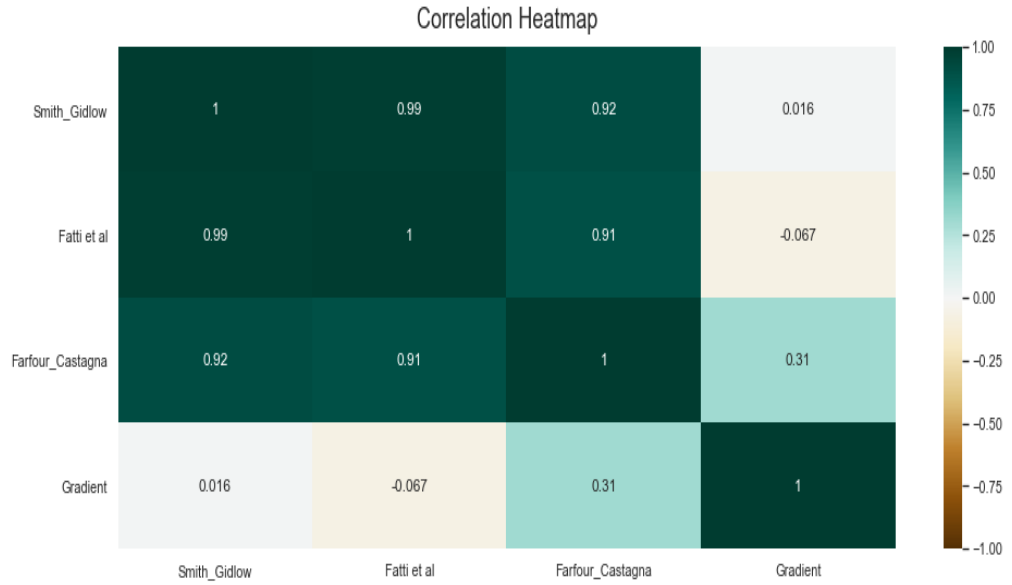

Fig. 3 Correlation Heatmap showing the correlation coefficient between fluid factors

The Heatmap in Figure 3 presents the correlation between FF1, FF2, and FF3. The map infers that the similarity is quite high between FF1 and FF2. FF3 has high correlation with FF1 and FF2 but less than the correlation between FF1 and FF2. The high correlation confirms that FF3 conveys different, or differently weighted, information than FF1 and FF2. It worth noting that FF3 shows more dependence on the Gradient than other attributes do.

Figures 4 and 5 depict the results of the application of the three attributes on the data samples. The fluid attributes exhibit different rates of success in detecting hydrocarbon-saturated sands and discriminating them from shale and brine sands for which almost all cases exhibit negative amplitudes (Fig. 04). For gas sand over brine sand interfaces, almost all attributes exhibit large positive amplitudes (Fig. 05). Lastly, at the shale over brine interfaces, we notice that different attributes have large differences (Figure 4). An explanation is that some of the brine sands have different Vp-Vs relationships than shales. Thus, they will not follow the same background line. Consequently, the fluid factors can show some false large anomalies (Fatti et al. 1994).

More importantly, we observe that FF3 could detect the reservoirs and distinguish them from brine in all the cases. In some cases, it shows better performance than FF1 and FF2. This might be due to the sensitivity of the Gradient to fluid, which represents 30% of FF3 sensitivity (see Figure 3).

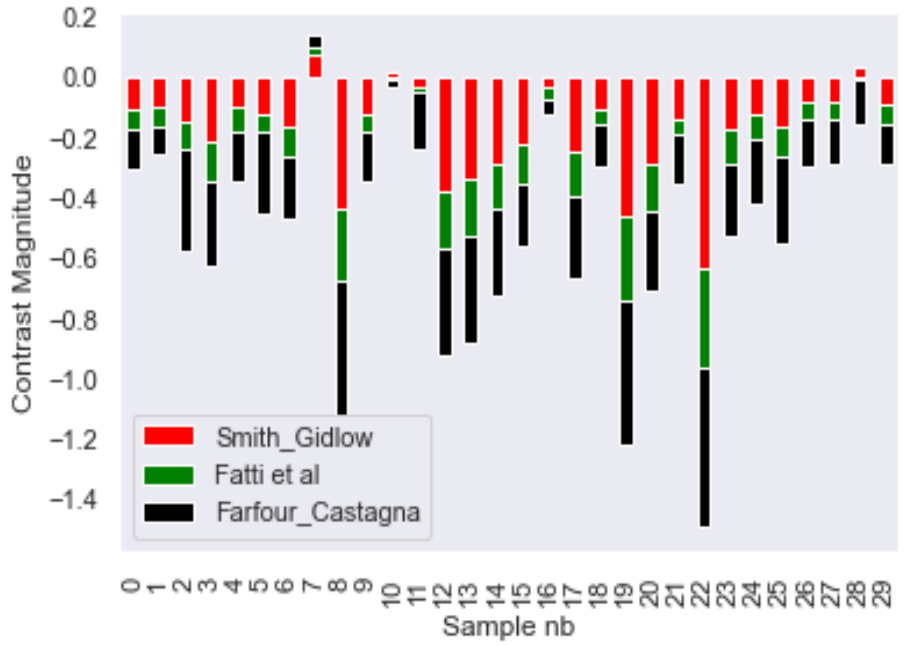

Fig. 4 Fluid attributes computed at shale/reservoir sands. The magnitude represents the contrast between the seal (shale) and the reservoir.

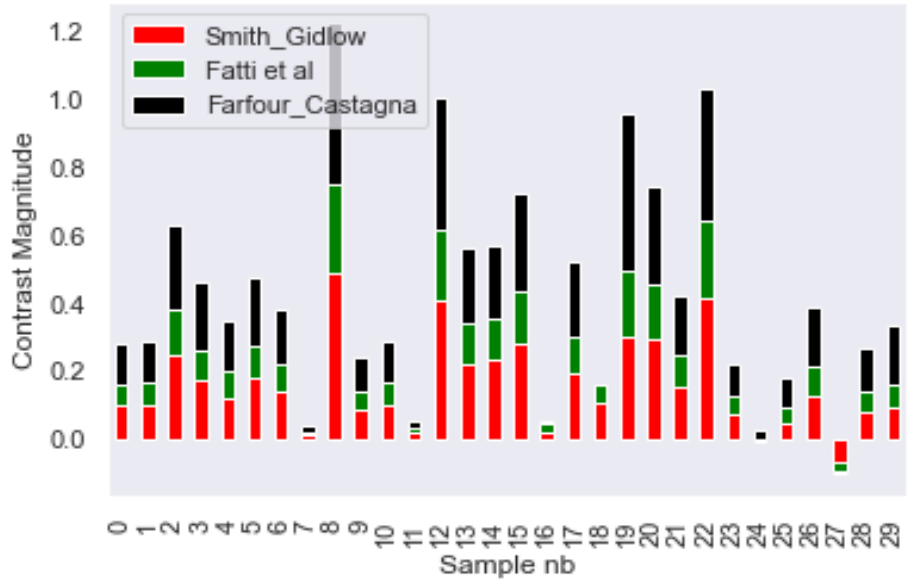

Fig. 5 Fluid attributes computed at reservoir/ brine sands. The magnitude represents the contrast between the reservoir and the brine sand.

4. Application to real data from North Western Australia

The data used in this section is from the Poseidon field, Browse Basin of North Western Shelf of Australia. The targeted reservoirs belong to the Plover Formation, which hosts major petroleum reservoirs in a number of fields. The Plover Formation is deposited in a fluvial-deltaic environment during early to middle Jurassic

(Tovaglieri and George, 2013). The seismic data polarity is SEG normal (hard interface is a positive). Three wells are used for calibration purposes namely, Poseidon 1, Poseidon 2, and Kronos 1. First, AVO modeling was performed at the well locations to predict the amplitude behavior at the top of the reservoirs. The modeling suggested that the reservoirs belong to Class II and Class IIp, (Rutherford and Williams, 1989; Ross and Kinman, 1995) a weak negative (sometimes positive) intercept and negative gradient.

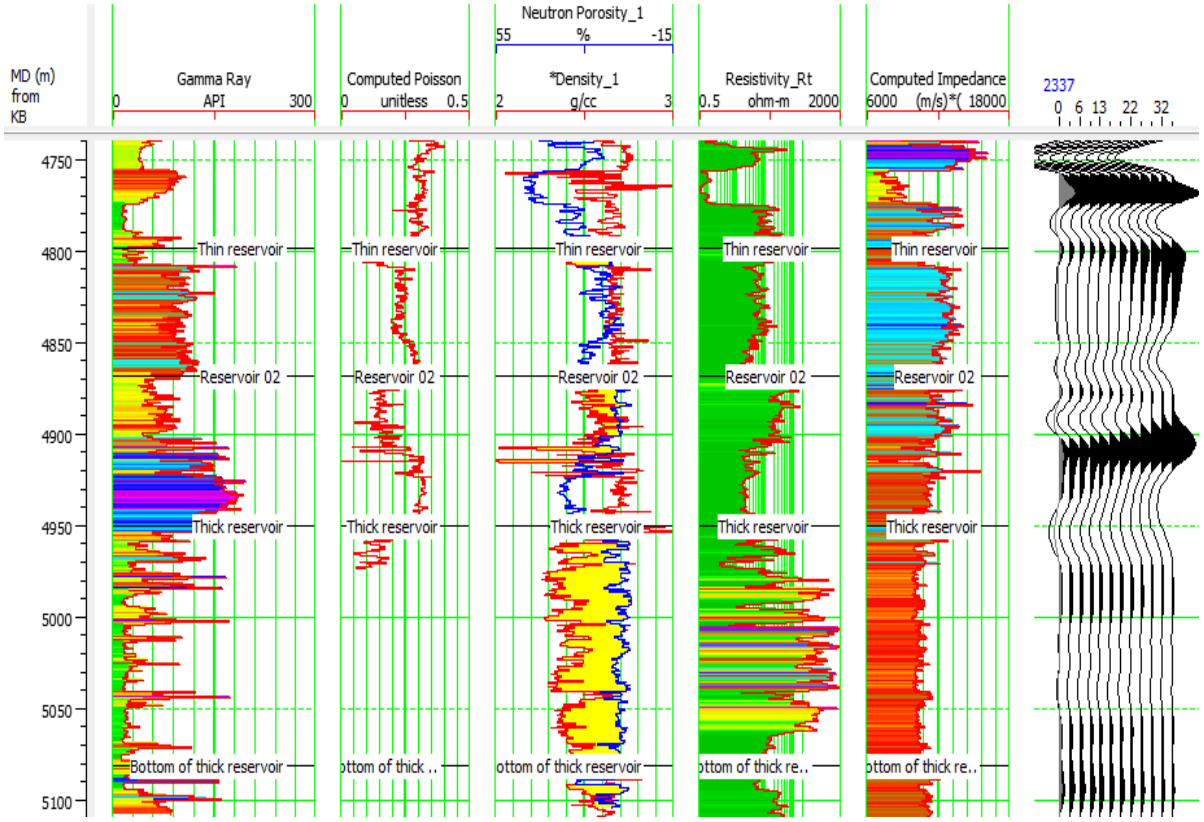

Fig. 6 Well logging data and synthetic traces computed at the well location.

After the AVO modeling, the fluid attributes were calibrated using data from the available wells. Figure 7 illustrates the performance of the attributes based on the provided Vp, Vs, density values from the calibration wells. The values are illustrated in Table 1.

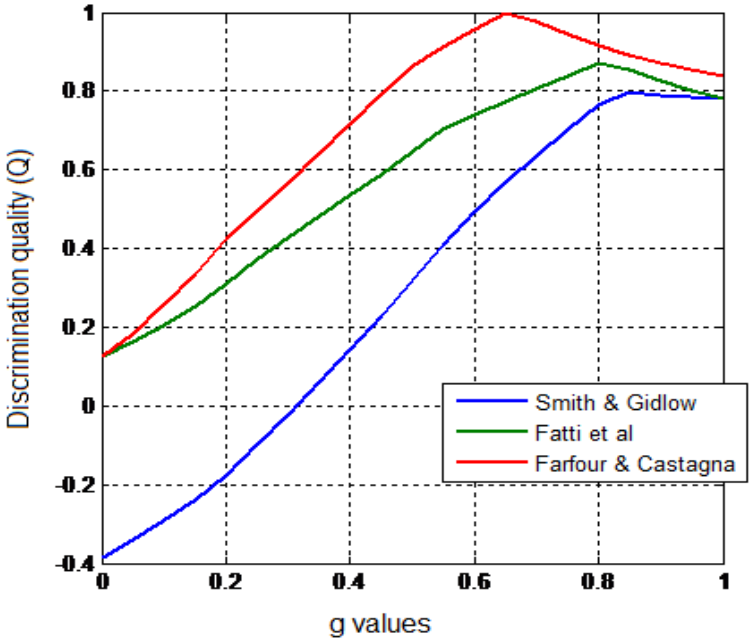

Fig. 7 Calibration of the fluid factor using data from local geology.

The figure indicates that FF3 petrophysically reaches its best discrimination capability when g is around 0.65 and should do so on real data if properly amplitude calibrated. However, FF1 and FF2 reach their best discrimination when g is 0.8 and 0.85 respectively.

Table 1: Vp, Vs, and density values used for the calibration of the fluid factors. The data are extracted from Poseidon 01, Boreas 01, Kronos 01. Note that Kronos 01 was used as blind well.

Seal			Gas-sand			Brine-sand		
Vp (km/s)	Vs (km/s)	Density (g/cc)	Vp (km/s)	Vs (km/s)	Density (g/cc)	Vp (km/s)	Vs (km/s)	Density (g/cc)
4.6	2.48	2.63	4.748	3.222	2.43	4.555	3.022	2.4
4.13	2.172	2.7	4.323	3.089	2.5	4.384	2.93	2.78
4.353	2.4	2.69	4.441	2.834	2.4	4.732	2.558	2.7
4.515	2.481	2.7	4.6	2.927	2.45	3.985	2.575	2.54
3.118	1.629	2.8	4.569	2.932	2.45	4.695	2.677	2.67
4.42	2.411	2.6	4.177	2.534	2.31	3.936	1.971	2.64

Next, the available partial stacks were subject to thorough preconditioning and random noise filtering to remove residual noises and improve data quality. Figure 7 shows a seismic section passing through the discovery well, Poseidon 1. Structural interpretation of the data showed that the reservoir zone is heavily affected by the different tectonic events that took place throughout geological times in the area. It was also

noticed that the regional seal above the zone of interest is characterized by very good continuity and stable seismic character. Seismically, the top of this Jamison shale is characterized by large positive amplitude. The partial stacks were used to produce angle gathers to perform the AVO analysis and compute the AVO attributes volumes.

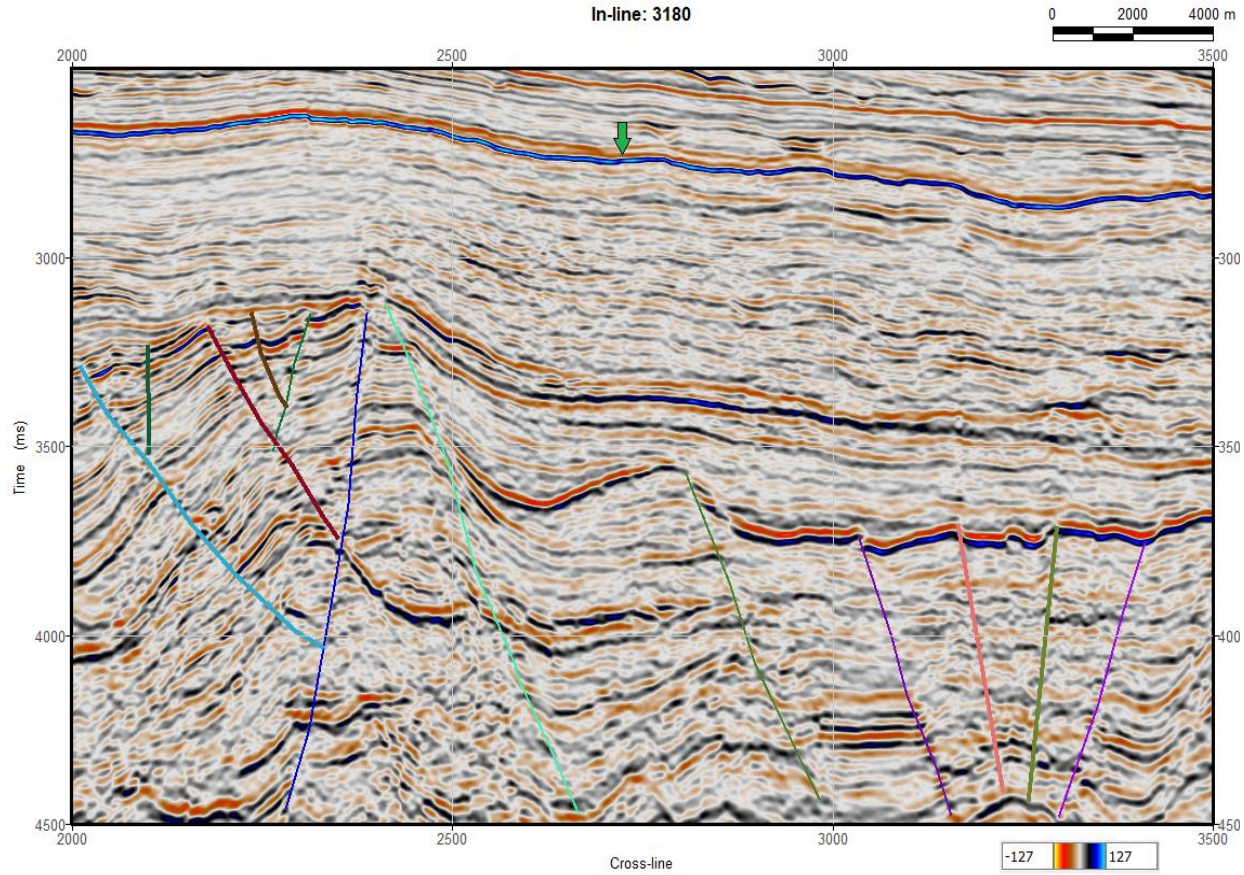

Fig. 8 A seismic section passing through the discovery well. The reservoir occurs at 3200ms. Jamison shale formation appears as a strong positive marker (marked with green arrow).

Figure 9 shows the intercept and gradient derived from the gathers. The attribute sections confirm the result of the AVO modeling. That is, the intercept section demonstrates that the reservoirs have low amplitude at normal incidence; while the gradient section shows that the reservoirs can be distinguished from their surrounding rocks by their amplitude variation.

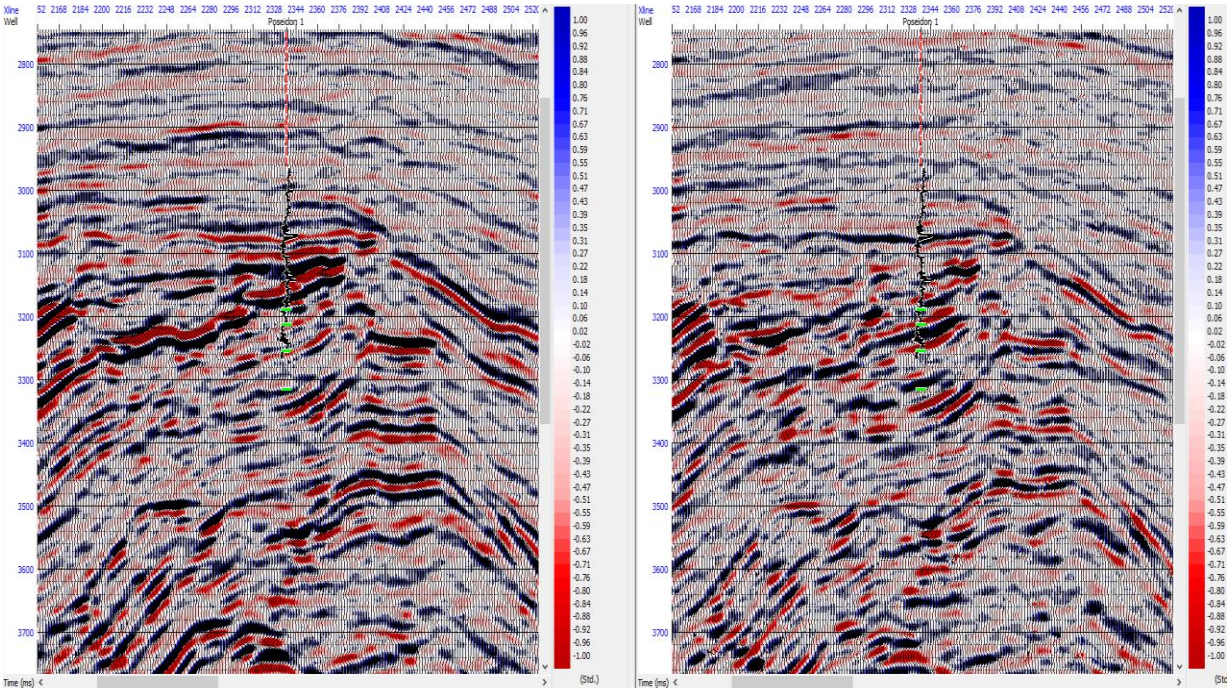

Fig. 9 Intercept and Gradient computed from the gathers. The inserted log in the figures is Vp/Vs ratio. The tops and bottoms of the reservoirs are marked in green.

Figure 10 shows the FF3 section derived from the intercept and gradient using equation 9. The calibration parameter determined from well data helped reduce the contribution of lithology and improve the fluid effect. The latter section shows appealing reflections at the top and at the bottom of the reservoirs much better than the intercept and gradient sections do. On the other hand, the Jamison shale formation appears as a very weak reflection, which vanishes at some parts of the section. All the above observations are found consistent with the definition of the fluid indicator (Castagna and Smith, 1994). The fluid factor was also tested over a section passing through Boreas 01 and similar results were obtained (Fig. 11). Next, FF3 was applied on a section passing by Kronos 01, which was not involved in the calibration and was used as blind well. The FF3 section infers a clear anomaly at the top of the reservoir that is weaker than the ones observed in the previous well. This is because the gas sand is thinner compared to the sand in Poseidon 01 and Boreas 01. This makes the gas effect on the amplitude less pronounced. Figure 12 displays the well logging data recorded at Kronos 01 along with FF3 traces computed at the well location. The well logging data confirm the interpretation of the results from the FF3 data. It is important to note that FF1 and FF2 have shown nearly the same fluid expressions.

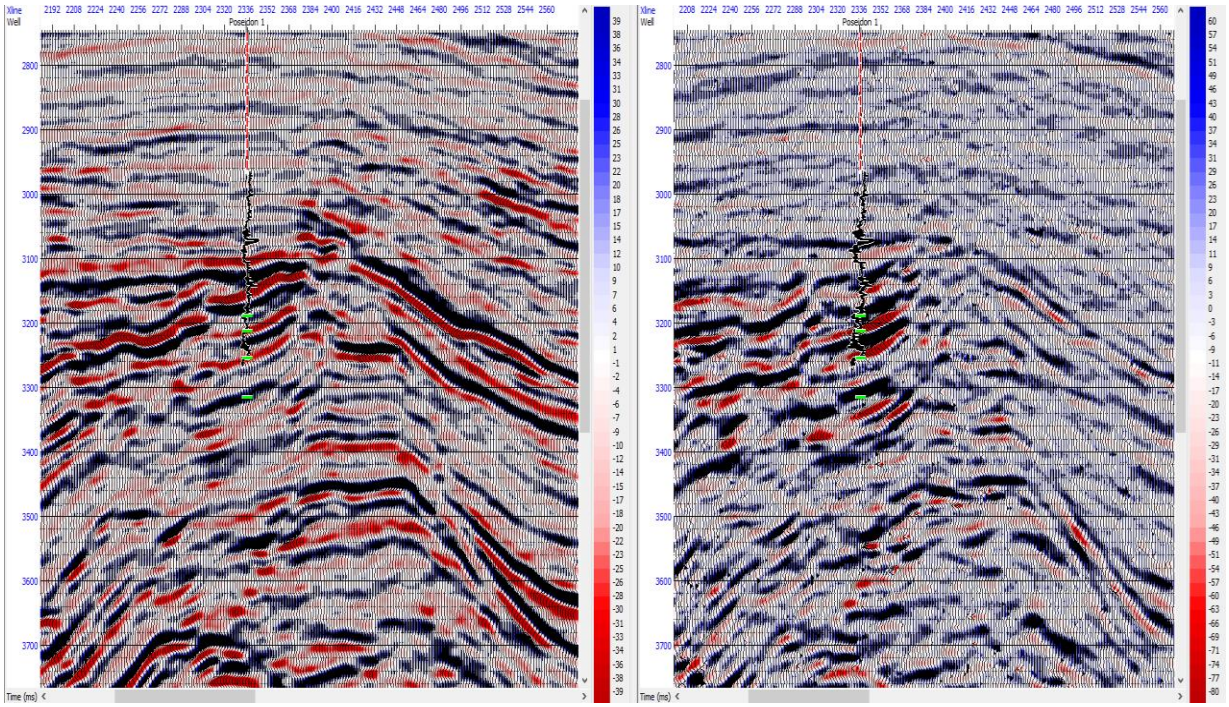

Fig. 10 Full stack and FF3 section crossing Poseidon 01 well. Top and base of the reservoir are marked in green.

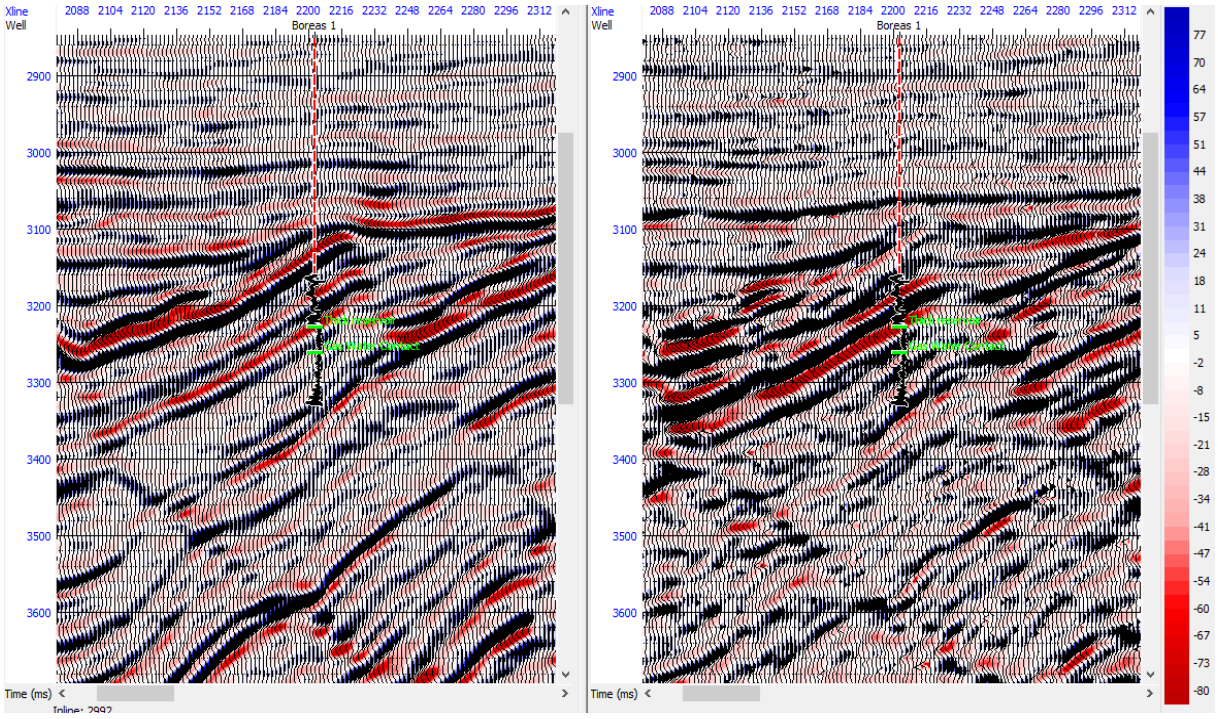

Fig. 11 Full stack and FF3 sections crossing Boreas 01 well. Top and base of the reservoir are marked in green.

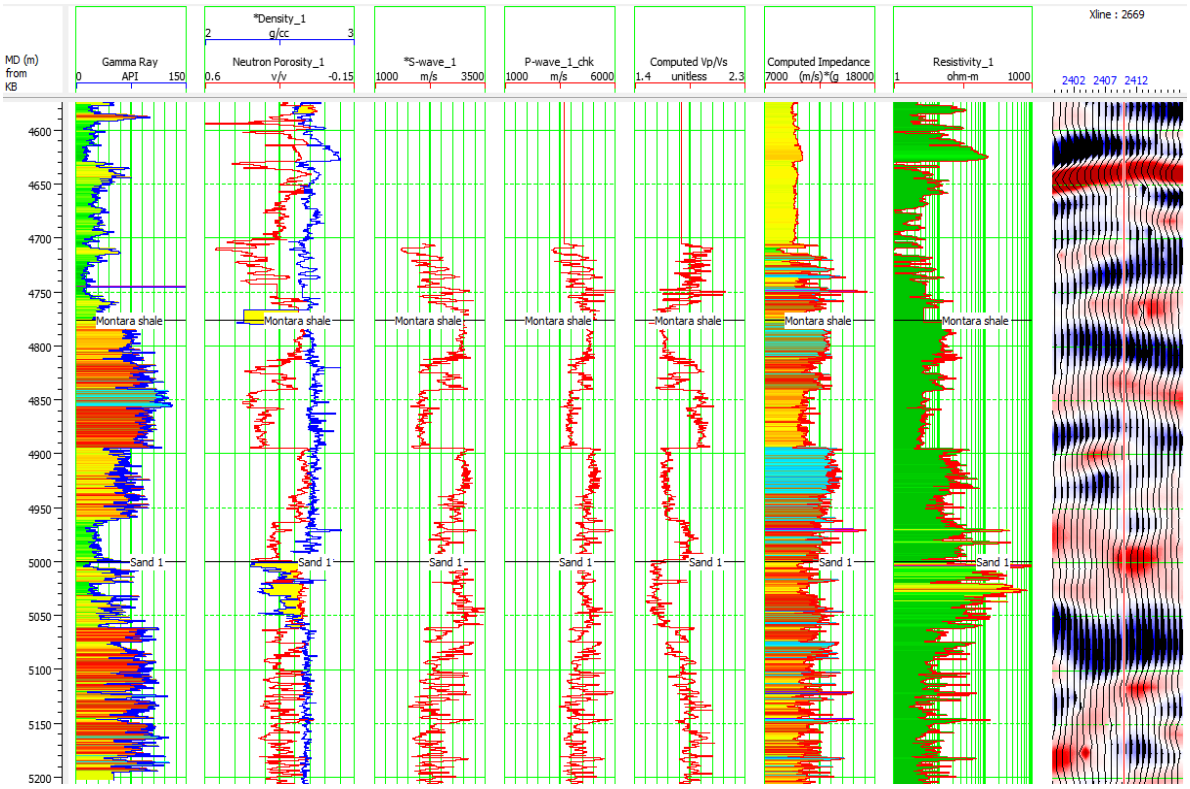

Fig. 12 Well logging data and FF3 computed at Kronos 01 (used as blind well).

For better analysis and interpretation, the attribute was extracted over a random line that crosses three wells (Fig 13). The random line gives a clear insight about the observed anomalies. The line shows also that there are other potential zones that are not drilled and can be considered as good prospects. The structural interpretation inferred that the anomalies terminate against clear sealing faults which is consistent with the structural and petroleum geology of the area.

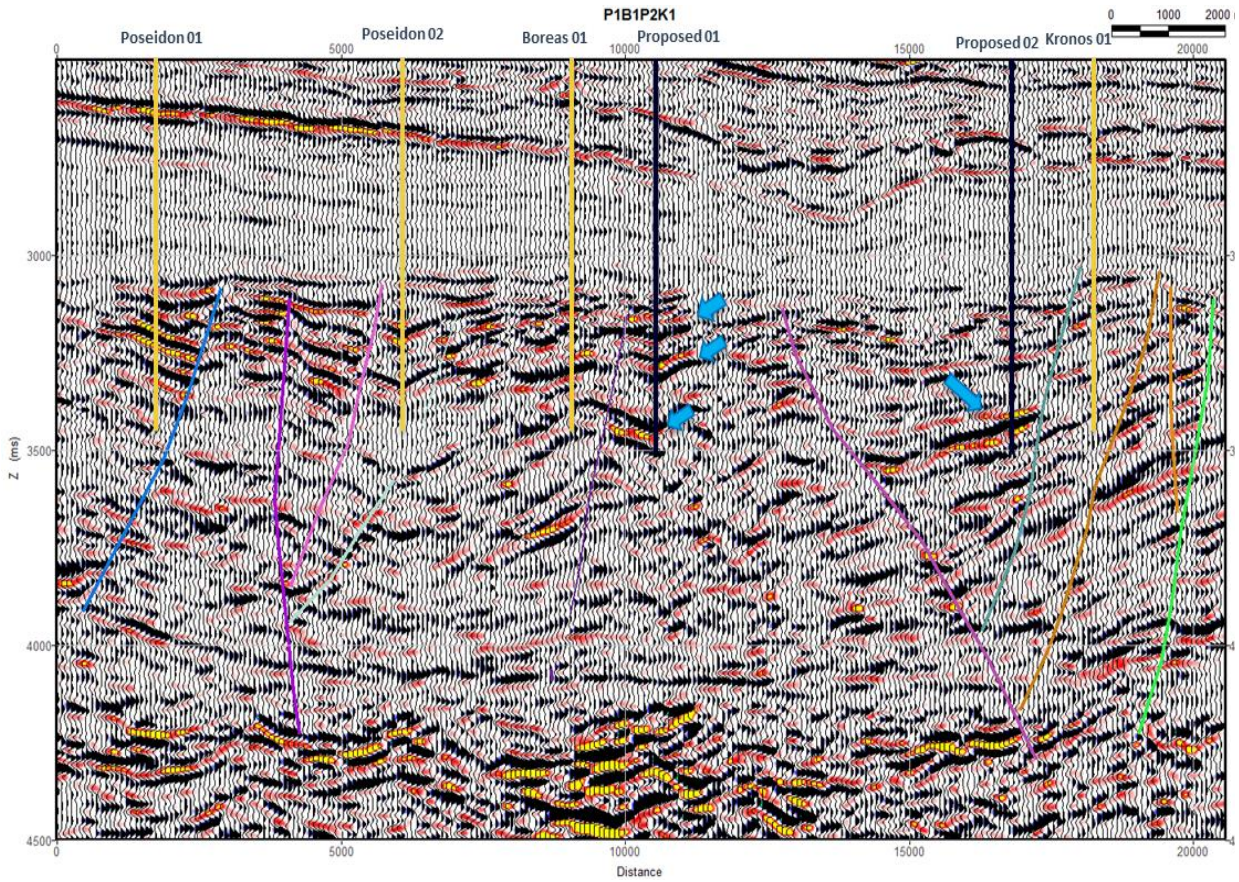

Fig 13. FF3 computed over a random lime passing by the gas producing wells (yellow). Potential zones (blue arrows) and proposed well locations (black) are marked on the section.

5. Conclusion:

In this study, a new expression of fluid factor is introduced. The proposed expression is a function of AVO intercept and gradient and a weighting parameter that depends on local geology. The new attribute is compared against existing fluid indicators and shows capability of detecting hydrocarbon-saturated reservoirs. We demonstrated that a good determination of the calibration factor, g, can help cancel the lithology contribution and correct amplitudes for other factors that are not considered in AVO reflectivity equations. The proposed AVO attribute was tested on real data from different world basins and on 3-D seismic data from North Western Australia. The attribute helped detect gas-saturated reservoirs and propose new potential zones. The findings from the attribute are found consistent with the petroleum geology of the area.

Acknowledgment

We would like to thank CeoSolutions for providing Hampson-Russell software and Geoscience Australia for providing the data used in this paper.

References

1. Aki, K., and Richards, P.G., 1980, Quantitative seismology: Theory and methods: W. H. Freeman and Co.
2. Bortfeld, R., 1961, Approximation to the reflection and transmission coefficients of plane longitudinal and transverse waves: Geophys. Prosp., **9**, 485-503.
3. Castagna, J. P., and Smith, S. W., 1994. Comparison of AVO indicators: A modeling study. Geophysics, 59**,** 1849–1855.
4. Castagna, J.P., Batzle, M.L., and Eastwood, R.L., 1985, Relationship between compressional-wave and shear-wave velocities in clastic silicate rocks: Geophysics, Vol. 50, p. 571-581
5. Domenico, S. N., 1977, Elastic properties of unconsolidated porous sand reservoirs: Geophysics, 42, 1339–1368, doi: https://doi.org/10.1190/1.1440797.
6. Farfour, M. (2020). Amplitude components analysis: Theory and application. The Leading Edge, 39(1), 62a1-62a6. https://doi.org/10.1190/tle39010062a1.1
7. Farfour, M. and Foster, D., 2021. New AVO expression and attribute based on scaled Poisson reflectivity. Journal of Applied Geophysics, 185, https://doi.org/10.1016/j.jappgeo.2021.104255.
8. Farfour, M., & Foster, D. (2022). Detection of hydrocarbon- saturated reservoirs in a challenging geological setting using AVO attributes: A case study from Poseidon field, Offshore Northwest region of Australia. Journal of Applied Geophysics, 203, 104687. https://doi.org/10.1016/j.jappgeo.2022.104687.
9. Farfour, M., Ferahtia, J., Djarfour, N., Aitouch, MA. (2018). Seismic spectral decomposition applications in seismic: A review and application. Oil and Gas Exploration: Methods and Application, 93-113. https://doi.org/10.1002/9781119227519.ch6
10. Fatti, J. L., G. C. Smith, P. J. Vail, P. J. Strauss, and P. R. Levitt, 1994. Detection of gas in sandstone reservoirs using AVO analysis: a 3-D seismic case history using the Geostack technique: Geophysics, 59, 1362–1376, doi: https://doi.org/10.1190/1.1443695.
11. Gray, D., 2002, Elastic inversion for Lamé parameters: SEG Technical Program, Expanded Abstracts, 213–216, doi: https://doi.org/10.1190/1.1817128.
12. Koefoed, O., 1955, On the effect of Poisson's ratios of rock strata on the reflection coefficients of plane waves: Geophysical Prospecting, 3, 381–387, doi: https://doi.org/10.1111/j.1365-2478.1955.tb01383.x.
13. Ostrander, W. J., 1984, Plane-wave reflection coefficients for gas sands at non-normal angles of incidence: Geophysics, 49, 1637–1648, doi: https://doi.org/10.1190/1.1441571.
14. Ross, C.P., and Kinman, D.L., 1995, Nonbright-spot AVO; two examples: Geophysics, 60, 1398-1408.
15. Rutherford, S.R., and Williams, R.H., 1989, Amplitude-versus-offset variations in gas sands: Geophysics, 54, 680-688.
16. Shuey, R. T., 1985, A simplification of the Zoeppritz equations: Geophysics, 50, 609–614, doi: https://doi.org/10.1190/1.1441936.
17. Smith, G. C., and R. A. Sutherland, 1996, The fluid factor as an AVO indicator: Geophysics 61, 1425–1428, doi: https://doi.org/10.1190/1.1444067.
18. Smith, G.C. and Gidlow, P.M., 1987, Weighted stacking for rock property estimation and detection of gas: Geophys. Prosp., **35**, 993-1014.

    Tovaglieri, F., and A. D. George, 2014, Stratigraphic architecture of an Early–Middle Jurassic tidally influenced deltaic system (Plover Formation), Browse Basin, Australian North West Shelf: Marine and Petroleum Geology, 49, 59–83, doi: https://doi.org/10.1016/j.marpetgeo.2013.09.011